PLOS Pathogens

RESEARCH ARTICLE

Antibiotic-resistance mutations in penicillin-binding protein 2 from the ceftriaxone-resistant *Neisseria gonorrhoeae* strain H041 strike a delicate balance between increasing resistance and maintaining transpeptidase activity

Marissa M. Bivins[1☯], Joshua Tomberg[1☯], Madeleine Bagshaw[2¤a], Avinash Singh[3¤b], Sandeepchowdary Bala[4], Christopher Davies[4]*, Robert A. Nicholas[1,5]*

1 Department of Pharmacology, University of North Carolina at Chapel Hill, Chapel Hill, North Carolina, United States of America, **2** Department of Biology, University of North Carolina – Chapel Hill, Chapel Hill, North Carolina, United States of America, **3** Department of Biochemistry & Molecular Biology, Medical University of South Carolina, Charleston, South Carolina, United States of America, **4** Department of Biochemistry & Molecular Biology, University of South Alabama, Mobile, Alabama, United States of America, **5** Department of Microbiology and Immunology, University of North Carolina at Chapel Hill, Chapel Hill, North Carolina, United States of America

☯ These authors contributed equally to this work.
¤a Current address: Department of Biological Sciences, Vanderbilt University, Nashville, Tennessee, United States of America
¤b Current address: Department of Biochemistry and Molecular Pharmacology, New York University Grossman School of Medicine, New York, United States of America
* cdavies@southalabama.edu (CD); nicholas@med.unc.edu (RAN)

Check for updates

OPEN ACCESS

Citation: Bivins MM, Tomberg J, Bagshaw M, Singh A, Bala S, Davies C, et al. (2026) Antibiotic-resistance mutations in penicillin-binding protein 2 from the ceftriaxone-resistant *Neisseria gonorrhoeae* strain H041 strike a delicate balance between increasing resistance and maintaining transpeptidase activity. PLoS Pathog 22(3): e1013721. https://doi.org/10.1371/journal.ppat.1013721

Editor: Alison K Criss, University of Virginia, UNITED STATES OF AMERICA

Received: November 11, 2025

Accepted: February 18, 2026

Published: March 17, 2026

Copyright: © 2026 Bivins et al. This is an open access article distributed under the terms of the Creative Commons Attribution License, which permits unrestricted use, distribution, and reproduction in any medium, provided the original author and source are credited.

Data availability statement: Data are available at the UNC Dataverse repository (https://doi.org/10.15139/S3/TEIYX2). The PDB codes of the crystal structures presented here are 9Z0W

Abstract

The mosaic *penA* allele (*penA41*) from H041, the most ceftriaxone-resistant *Neisseria gonorrhoeae* strain identified to date, encodes a variant of the essential Penicillin-Binding Protein 2 (PBP2) with 60 amino acid mutations compared to PBP2 from the antimicrobial-susceptible strain, FA19. Based on previous work from our lab and others, we identified a minimal set of 10 mutations that, when introduced into the β-lactam antibiotic-susceptible *penA* allele from FA19 (*penA19*), confers two-thirds of the ceftriaxone and cefixime resistance compared to the *penA41* allele. Three mutations (A311V, I312M, and V316P) are in the *α*2 helix of PBP2 containing the catalytic serine (Ser310), two (F504L and N512Y) are in the *β*3-*β*4 loop that is important in binding and acylation, and one (G545S) interacts with conserved amino acids in the active site. The seventh mutation, T483S, confers substantial resistance to ceftriaxone within the minimal mutant set but requires the presence of three epistatic mutations located on the other side of the protein that do not alter resistance on their own yet are necessary to retain essential function. These epistatic mutations change the backbone dihedral angles at position-447, which may increase flexibility of the enzyme and help maintain enzymatic function. Our results highlight the complex balance necessary for evolving cephalosporin

(tPBP2-6M), 9Z0X (tPBP2-7M), and 9Z0Y (tPBP2-10M) and are available at the link above and at RCSB.org.

Funding: This study was supported by the National Institute for General Medical Sciences award GM66861 (C.D. and R.A.N.) and the National Institute for Allergy and Infectious Diseases awards AI164794 (C.D. and R.A.N.) and U19 AI113170 (R.A.N.). The sponsors/funders did not play any role in the study design, data collection and analysis, decision to publish, or preparation of the manuscript.

Competing interests: The authors have declared that no competing interests exist.

resistance in PBP2 while also retaining sufficient transpeptidase function to support growth.

Author summary

In this study, we set out to understand how *Neisseria gonorrhoeae*, the bacterium that causes gonorrhea, is able to resist the last remaining recommended antibiotic, ceftriaxone. Gonorrhea is a common sexually transmitted infection worldwide, and rising resistance threatens to make it untreatable. We focused on penicillin-binding protein 2 (PBP2), which is essential for the bacterium's survival and is the lethal target of ceftriaxone. By incorporating a subset of the 60 PBP2 mutations found in a highly resistant strain into PBP2 from an antibiotic-susceptible strain, we discovered that resistance evolved from a combination of mutations that work together to directly reduce the capacity of ceftriaxone to inactivate the protein and others that act as "supporting" mutations to keep the protein functional despite the presence of the resistance mutations. Our study highlights how *N. gonorrhoeae* successfully negotiates the delicate balance between resistance and function to escape the lethal action of antibiotics.

Introduction

Neisseria gonorrhoeae is a Gram-negative bacterium that causes the sexually transmitted infection (STI), gonorrhea. The World Health Organization (WHO) reported an estimated 82 million gonorrhea cases globally in 2019 [1] and the Centers for Disease Control and Prevention (CDC) reported that gonorrhea is the second most prevalent STI in the United States, with over 600,000 cases reported in 2023 [2]. The actual number of gonorrhea cases is likely to be much higher, since 7% to 15% of infections in men and 16% to 70% of infections in women are asymptomatic [3–5]. Prolonged *N. gonorrhoeae* infections can result in serious complications, including pelvic inflammatory disease, infertility, and increased susceptibility to HIV infection [6–8]. Currently, the only recommended treatment by the CDC for gonorrhea is a single 500 mg injection of the extended spectrum cephalosporin (ESC), ceftriaxone, but resistance to this β-lactam antibiotic is on the rise [9–13].

The targets for β-lactam antibiotics such as ceftriaxone are the penicillin-binding proteins (PBPs), which synthesize and cross-link the peptidoglycan layer that surrounds bacteria [14,15]. *N. gonorrhoeae* has two essential PBPs: PBP1 and PBP2 [16,17]. PBP1 is a class A bifunctional PBP that catalyzes both glycan polymerization and crosslinking of the peptide strands of peptidoglycan, whereas PBP2 is a class B monofunctional PBP that cross-links peptide strands during cell division but requires a partner protein, FtsW, for glycan polymerization [18–20]. Peptidoglycan crosslinking occurs through transpeptidation, in which the PBPs form an acyl-enzyme complex with the penultimate D-Ala from the acyl-D-Ala-D-Ala C-terminus of the peptidyl chain

and then reacts with the free amino group in *m*-diaminopimelic acid (*m*-DAP) from a parallel peptidoglycan strand, forming a cross-link and releasing the enzyme to catalyze another round. β-lactam antibiotics target PBPs by mimicking the acyl-D-Ala-D-Ala C-terminus of the peptide chains and forming a long-lived acyl-enzyme complex with the PBP [14,15,21,22].

Of the two essential PBPs, PBP2 historically has had a much higher rate of acylation than PBP1 with essentially all β-lactam antibiotics used to treat gonococcal infections, making PBP2 the lethal target of these antibiotics [16,23,24]. During the four decades when penicillin was used to treat infections, the *penA* gene encoding PBP2 acquired mutations comprising an amino acid insertion (Asp345a) and four to eight mutations in the C-terminus of the PBP, with the insertion and the C-terminal mutations contributing equally to decreasing the acylation rate [24,25]. Following the removal of penicillin, the ESCs ceftriaxone and cefixime were used extensively to treat gonorrhea, but strains emerged from East Asia in the early 2000s with decreased susceptibility to ESCs [26–28]. Unlike penicillin-resistant strains, these isolates had so-called mosaic *penA* alleles, in which segments of *penA* genes from other *Neisseria* species were recombined into *N. gonorrhoeae penA*, resulting in PBP2 variants with 40–60 mutations compared to PBP2 from susceptible strains [26,29]. These mosaic alleles emerged as a result of *N. gonorrhoeae* being naturally competent, which facilitates the uptake and recombination of closely related DNA into its genome by homologous recombination. This property allows for both the original formation of the mosaic alleles (a low frequency event) and the spread of these alleles in the population (high frequency), provided that these genes do not have a large fitness cost.

One example of a strain with a mosaic *penA* allele is H041 (referred to hereafter as *penA41*), which was isolated in Japan in 2009 and has the highest level of resistance to ceftriaxone (MIC = 2–4 μg/mL) and cefixime (MIC = 8 μg/mL) of any gonococcal isolate to date [30,31]. Compared to PBP2 from an antibiotic-susceptible isolate, e.g., FA19 ($PBP2^{FA19}$), PBP2 from H041 ($PBP2^{H041}$) has 60 amino acid alterations [30]. To understand how these mutations decrease the capacity of PBP2 from ESC-resistant strains to be inhibited by ESCs, we previously solved crystal structures of the transpeptidase domains of $PBP2^{FA19}$ and $PBP2^{H041}$ (denoted by the prefix t) and found that conformational changes observed in $tPBP2^{FA19}$ after acylation by ceftriaxone and ceftriaxone do not occur in $tPBP2^{H041}$ [32,33]. These changes include movement of the *β*3-*β*4 loop towards the active site, where it forms contacts with other residues in PBP2 and with the R_1 moieties of ESCs, and twisting of the *β*3 strand, which contains the highly conserved KTG motif [22,34], towards the active site to aid in formation of the oxyanion hole that stabilizes the tetrahedral transition state during acylation [32,33].

In previous studies, we and others have identified seven mutations that are important in conferring resistance: A311V, I312M, V316P, T483S, F504L, N512Y, and G545S (Fig 1) [35–38]. Understanding how these seven mutations work together to impact both antibiotic resistance and strain fitness is vital for understanding *N. gonorrhoeae* evolution more broadly and for developing new therapeutics. We grouped these seven mutations from the *penA41* allele of H041 into three clusters based on their location in the protein and examined their effects on the MICs of ESCs and penicillin G by either incorporating them into the *penA* allele from FA19 (*penA19*) in the absence of other mutations or reverting them to their *penA19* counterparts within the *penA41* background. Each group of mutations had varied effects depending on the antibiotic and the PBP2 background. We also attempted to incorporate all seven mutations together into *penA19* to create a "minimal mutant" that would confer the maximum level of resistance to FA19 after transformation. However, one of the mutations, T483S, was found to disrupt transpeptidase function, and required the presence of three non-resistance mutations (referred to as epistatic mutations) to support growth. When the seven mutations and three epistatic mutations were incorporated into the *penA19* background and transformed into FA19, they conferred 67% of the MICs of both ceftriaxone and cefixime relative to FA19 *penA41*. Crystal structures of the mutants reveal that the epistatic mutations change only the backbone dihedral angles at position 447, which may impart increased flexibility to the enzyme containing the resistance mutations. These data provide insight into how PBP-mediated resistance arises and how resistance mutations combine to increase resistance. They additionally highlight the delicate balance between increasing resistance and preserving essential function.

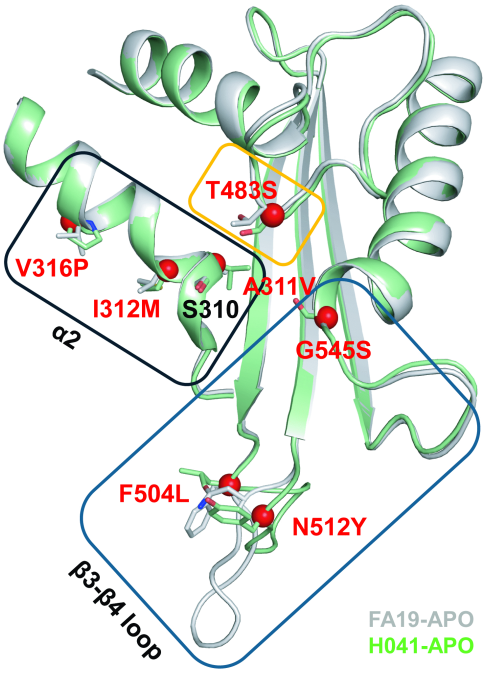

Fig 1. Mutations in PBP2 that confer ESC resistance to *N. gonorrhoeae*. A superimposition of two *apo* PBPs structures in the active site region is shown in ribbon format, where tPBP2^{FA19} (6P53) is colored grey and tPBP2^{H041} (6VBC) is green. Boxes indicate the groups of mutations that were analyzed in this study. The side chains of the amino acids of PBP2^{FA19} and PBP2^{H041} corresponding to the seven resistance mutations are shown in stick form and colored according to structure. Red spheres indicate the alpha carbon position of these residues in PBP2^{H041}. The Ser310 nucleophile is also shown.

https://doi.org/10.1371/journal.ppat.1013721.g001

Results

In previous studies, we and others identified seven mutations in mosaic PBP2 variants that confer resistance to the ESCs ceftriaxone and cefixime [33,35–38]. These mutations are clustered around the active site and can be grouped based on their location and/or effects on conformation: a) two *β*3-*β*4 loop mutations (F504L/N512Y) and G545S, b) three mutations (A311V/I312M/V316P) located on the same *α*2 helix as the active site Ser310 nucleophile, and c) the T483S mutation at the top of the active site (Fig 1). However, it is unclear whether these mutations act independently or not to decrease acylation with specific β-lactam antibiotics. To investigate potential dependencies, we introduced each of the groups of mutations into the *penA* gene from FA19 (*penA19*) or reverted them back to their *penA19* counterparts in the *penA* gene from H041 (*penA41*), transformed the mutant alleles into the antibiotic-susceptible strain, FA19, and determined the MICs of ceftriaxone, cefixime, and penicillin G.

*β*3-*β*4 loop mutations work in tandem with G545S to elevate MICs of ESCs

Introduction of either F504L/N512Y or G545S into *penA19* increases the MICs of ceftriaxone (MIC_{CRO}) and cefixime (MIC_{CFX}) by 1.5- to 3-fold, with G545S having a greater impact on the MICs than the *β*3-*β*4 loop mutations (Fig 2A). When all three mutations were introduced together, the MIC_{CRO} and MIC_{CFX} increased 3.5-fold and 6-fold, respectively, compared to *penA19*. Surprisingly, these mutations had no impact on the MIC of penicillin G (MIC_{PEN}).

Reverting these codons to their *penA19* equivalents in *penA41* showed a similar pattern, again with antibiotic-specific effects (Fig 2B). Reverting Ser545 to Gly in *penA41* results in a larger decrease in the MIC_{CRO} and MIC_{CFX} than does reversion of the two *β*3-*β*4 loop mutations. In contrast, reversion of Ser545 back to Gly had no effect on

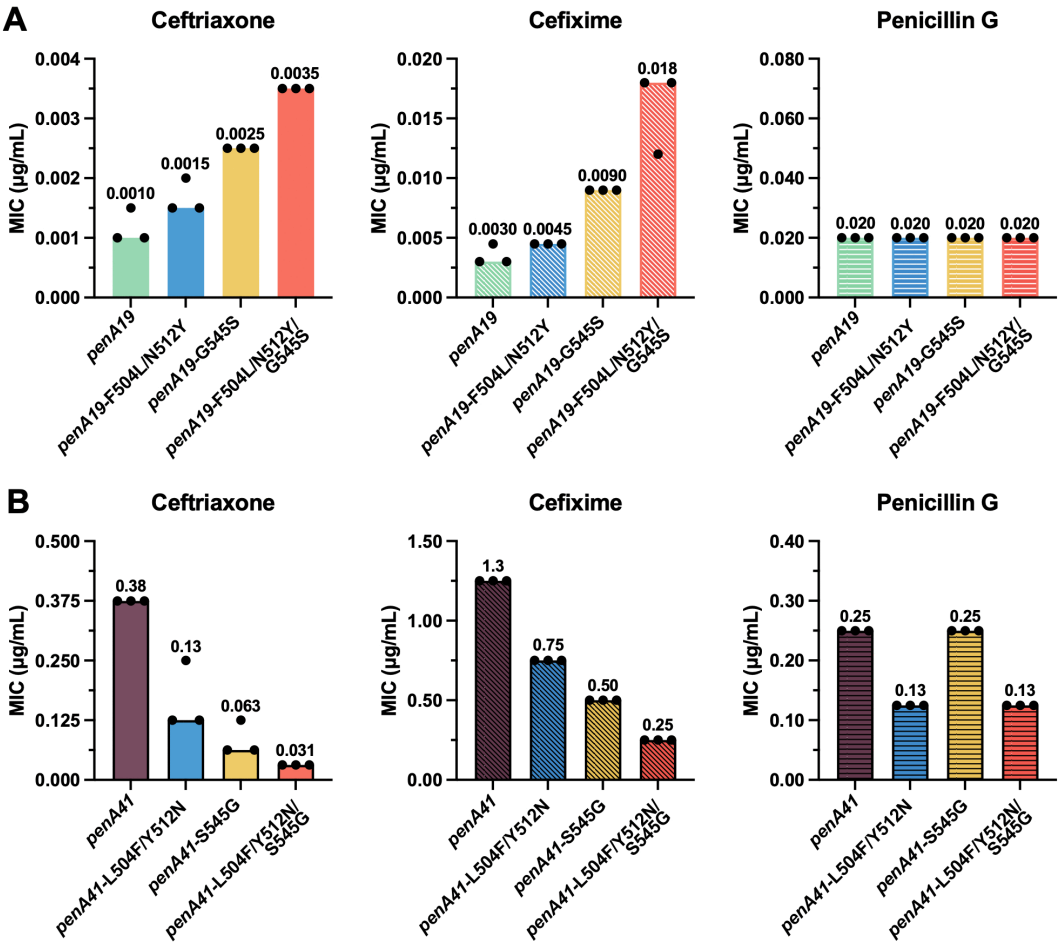

Fig 2. Effects of β3-β4 loop mutations and G545S on antibiotic MICs. MIC values of ceftriaxone, cefixime, and penicillin G in FA19 strains transformed with *penA19* containing the specified mutations from *penA41* (forward; **A**) or reversion of these mutations in *penA41* back to their counterparts in *penA19* (reversion; **B**). The bars represent the median MICs with individual replicates shown as points (n = 3).

https://doi.org/10.1371/journal.ppat.1013721.g002

MIC_{PEN}, whereas reverting the *β*3-*β*4 loop mutations decreased MIC_{PEN} twofold. When compared to *penA41,* the MIC_{CRO} was decreased the most (12-fold) when all three mutations were reverted, followed by MIC_{CFX} (5-fold), and MIC_{PEN} (2-fold).

Mutation and reversion of *α*2 helix amino acids markedly impact the MICs of ceftriaxone, cefixime, and penicillin G

Because of their proximity to one another, the three *α*2 mutations were mutated as a group to assess their contribution to ceftriaxone, cefixime, and penicillin G resistance. Mutation of the three codons to their *penA41* equivalents in *penA19* and transformation into FA19 increased the MIC_{CRO} and MIC_{CFX} by 5- and ~7-fold, respectively, compared to FA19, but had little to no impact on the MIC_{PEN} (Fig 3). In contrast, reverting these mutations to their *penA19* counterparts in the *penA41* background had a marked impact on the MICs of all three antibiotics tested, with the MICs for ceftriaxone, cefixime, and penicillin G decreased by 6-fold, 15-fold, and 6-fold, respectively (Fig 3). Notably, reversion of the three *α*2 mutations in *penA41* decreased the MIC_{PEN} to the same level as FA19.

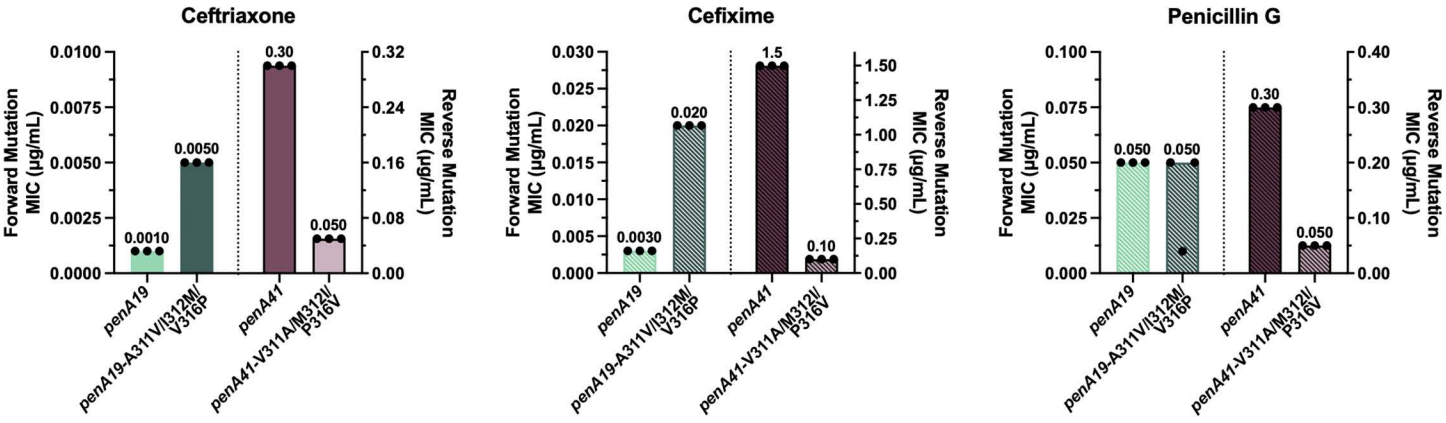

Fig 3. MIC values of ceftriaxone, cefixime, and penicillin G for FA19 strains transformed with *penA19* containing the *α*2 mutations from *penA41* (left side of each panel) or *penA41* containing reversions of amino acids 311, 312, and 316 to their counterparts in *penA19* (right side of each panel). Note that the left sides of each panel have a different Y axis than the right sides, due to the large differences in MICs of the antibiotics for the strains. The bars represent the median MICs with individual replicates shown as points (n = 3).

https://doi.org/10.1371/journal.ppat.1013721.g003

T483S disrupts the function of PBP2^{FA19} without three epistatic mutations

The T483S mutation sits at the top of the active site (Fig 1) and plays an important role in resistance in H041 and other high-level ESC-resistant strains such as FC428 [37,39]. In ESC-bound crystal structures of tPBP2^{H041} and tPBP2^{FA19}, the Ser or Thr side chain at position 483 projects toward ceftriaxone, though does not form a direct contact with the antibiotic in either structure [32, 33]. We mutated Thr483 to Ser in *penA19* and attempted to transform FA19, but no colonies were obtained despite repeated attempts. In contrast, reversion of Ser483 to Thr in the *penA41* background generated colonies and the MIC_{CRO} was decreased by 4-fold, along with MIC_{CFX} and MIC_{PEN} by 2- and 1.5-fold, respectively (Fig 4).

To measure of how much of the resistance to ESCs conferred by the full *penA41* allele depends on these seven identified resistance mutations, we initially introduced the two *β*3-*β*4 loop mutations, G545S, and the three *α*2 mutations into *penA19* (referred to as *penA19*-6M), transformed the construct into FA19, and determined the MICs of the three β-lactam antibiotics. For the ESCs, the MIC_{CFX} reached 33% of that conferred by the *penA41* allele in FA19, whereas the MIC_{CRO} and MIC_{PEN} reached 25% and 16% of that conferred by *penA41*, respectively (Fig 5). Unexpectedly, when we added the T483S mutation to *penA19*-6M (termed *penA19*-7M) and transformed it into FA19, only a few colonies were obtained on selection plates and all lacked the T483S mutation, suggesting that in the *penA19*-7M background, the T483S mutation disrupted the essential transpeptidase function of PBP2 to nonviable levels. This conclusion also was consistent with the inability to select for strains harboring *penA19*-T483S described above.

We surmised that some of the other mutations in *penA41* were important in preserving transpeptidase function in the presence of T483S. In previous studies on PBP2 from an ESC-reduced susceptibility *N. gonorrhoeae* strain (35/02) and ESC-resistant H041, we had divided the linear sequence into 6 modules (S1 Fig) to assess their contributions to resistance [36,37] and a similar approach was used here to identify these additional mutations. When the various modules (mods) from *penA41* were inserted into *penA19*-7M, only mod3^{H041} produced transformants. Sequencing of isolates confirmed that all seven of the resistance mutations, including T483S, were intact. Mod3 encompasses residues 432–489 and contains T483S as well as 12 additional mutations (S1 Fig). By trial and error (see S1 Text, S1 Fig, and S1 Table for a detailed description of these experiments), we winnowed down the twelve mod3^{H041} mutations to three-A437V, L447V, and F462I-that together supported growth in *penA19*-7M (this construct is referred to as *penA19*-10M). Mapping these onto the structure of PBP2 shows they are relatively distant from the active site region

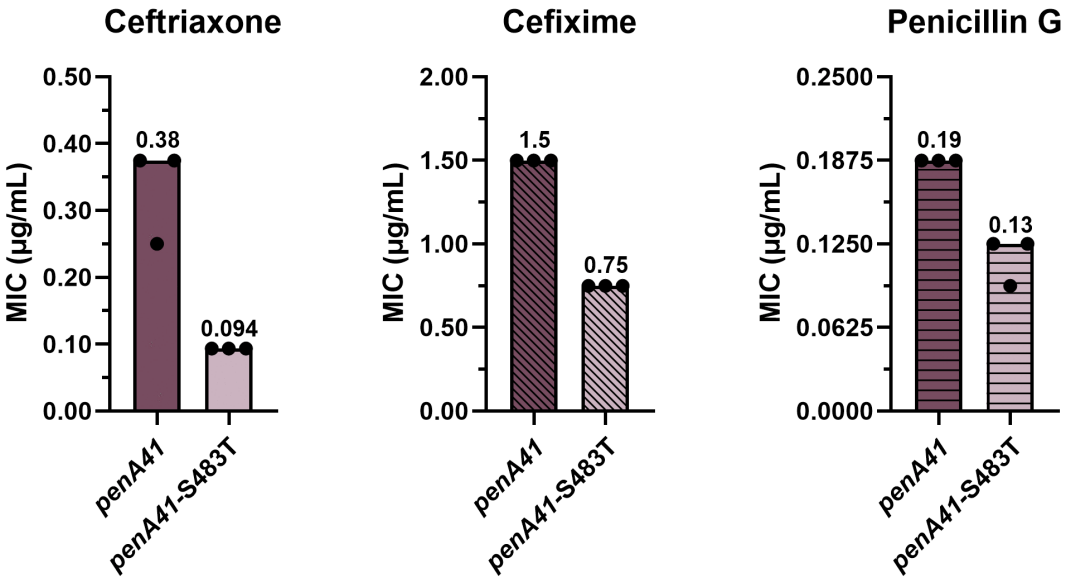

Fig 4. MIC values of ceftriaxone, cefixime, and penicillin G for FA19 strains transformed with *penA41* containing an S483T reversion. The bars represent the median MICs with individual replicates shown as points (n = 3).

https://doi.org/10.1371/journal.ppat.1013721.g004

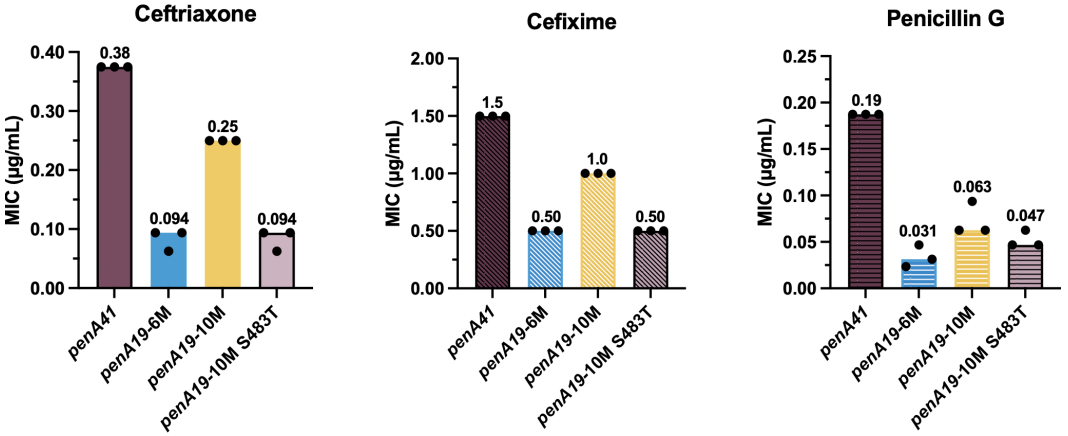

Fig 5. MIC values of ceftriaxone, cefixime, and penicillin G for FA19 strains transformed with *penA19* alleles containing multiple resistance mutations from *penA41*. The *penA19*-6M allele includes F504L, N512Y, G545S, A311V, I312M, and V316P resistance mutations. The *penA19*-10M allele contains all of the mutations in *penA19*-6M, plus T483S and the 3 epistatic mutations, A437V, L447V, and F462I. The bars represent the median MICs with individual replicates shown as points (n = 3).

https://doi.org/10.1371/journal.ppat.1013721.g005

(Fig 6). The MICs of ceftriaxone and cefixime for FA19 *penA19*-10M reached ~67% of that of FA19 *penA41*, with a more moderate impact on the MIC_{PEN} (Fig 5). Importantly, when Ser483 in *penA19*-10M was reverted to Thr and transformed into FA19 (*penA19*-10M S483T), the MICs of ceftriaxone and cefixime decreased to the same level as that conferred by *penA19*-6M (Fig 5). Taken together, these data suggest that the A437V, L447V, and F462I mutations have an epistatic effect on the T483S mutation, meaning that they do not contribute to resistance to ESCs but are required for the *penA19*-7M mutant to be viable.

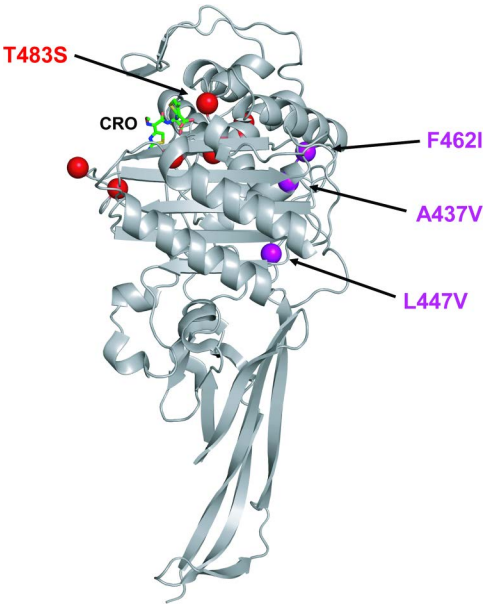

Fig 6. Location of the three epistatic mutations (purple spheres) and the seven resistance mutations (red spheres) in the ceftriaxone-bound tPBP2^{FA19} (6P54) structure. CRO indicates the location of ceftriaxone (green bonds) bound in the active site.

https://doi.org/10.1371/journal.ppat.1013721.g006

Acylation kinetics of PBP2 variants

To assess the *in vitro* effects of T483S on antibiotic binding to PBP2 in the presence or absence of the three epistatic mutations, we determined the k_2/K_s values of ceftriaxone, cefixime, and penicillin G for PBP2-6M, PBP2-7M, and PBP2-10M using purified proteins and compared them to previously reported values for PBP2^{FA19} and PBP2^{H041}. As shown in Table 1, the three antibiotics have extremely high k_2/K_s values for PBP2^{FA19}, whereas these values are markedly lower for PBP2^{H041}, consistent with their respective MICs for FA19 and H041. The k_2/K_s values of penicillin G, ceftriaxone, and cefixime are decreased by 38-fold, 620-fold, and 84-fold, respectively, for PBP2-6M relative to those for PBP2^{FA19}, and adding the T483S mutation (PBP2-7M) lowers them by another 7- to 13-fold. The k_2/K_s values of the three antibiotics for PBP2-10M are very similar to those for PBP2-7M, consistent with the lack of an effect of epistatic mutations on antibiotic binding.

The three epistatic mutations are insufficient to support cell growth when incorporated into *penA19*-T483S

The data detailed above suggest that one potential reason we could not select colonies following transformation of *penA19*-T483S into FA19 was because the inclusion of T483S disabled the essential transpeptidase activity of PBP2.

TABLE 1. k_2/K_s constants of Penicillin G, Ceftriaxone, and Cefixime for PBP2-6M, PBP2-7M, and PBP2-10M. k_2/K_s values were derived using [^{14}C]benzyl penicillin G as described in [24]. [a]Data from [37].

	k_2/K_s ($M^{-1}s^{-1}$)		
PBP2 Protein	**Penicillin G**	**Ceftriaxone**	**Cefixime**
[a]PBP2^{FA19}	75,700 ± 2,300	1,710,000 ± 90,000	1,480,000 ± 22,000
PBP2-6M	2,000 ± 43	2,745 ± 140	17,550 ± 644
PBP2-7M	285 ± 15	305 ± 7	1,343 ± 54
PBP2-10M	352 ± 12	483 ± 24	2,103 ± 45
[a]PBP2^{H041}	741 ± 28	135 ± 21	55 ± 14

https://doi.org/10.1371/journal.ppat.1013721.t001

We tested this idea by introducing the three epistatic mutations into *penA19*-T483S and transforming the construct into FA19. We obtained a small number of transformants (eight total in two experiments), but while we were able to incorporate the T483S mutation into FA19, all the transformants surprisingly also contained a spontaneous R502H mutation. Arg502 is 100% conserved in all sequenced *penA* alleles in *N. gonorrhoeae* [40], is located next to the highly conserved KTG sequence motif (residues 497–499) on the β3 strand [22], and contacts both ceftriaxone and cefixime in the acylated structures of tPBP2^{H041} [32,33,38]. Thus, even with the three epistatic mutations present, an additional non-native mutation (R502H) is necessary for the T483S mutation to maintain sufficient transpeptidase activity for growth in the *penA19* background.

The three epistatic mutations correlate with T483S in *Neisseria* species

Given the severe effects of the T483S mutation on strain viability, we examined its prevalence in *N. gonorrhoeae*, *N. meningitidis*, and commensal *Neisseria* species in the PubMLST database [40]. In *N. gonorrhoeae*, 0.7% (216 out of 32,719) of genomes within the database contained the T483S variant, likely representing strains with mosaic *penA* alleles. *Neisseria meningitidis*, the etiological agent of meningococcal disease, has less ESC-reduced susceptibility than *N. gonorrhoeae*, but recent studies have documented the emergence of such strains [41,42]. In the PubMLST database, 0.07% (34 out of 45,753) of meningococcal genomes contained the T483S mutation. Because mosaic *penA* alleles are known to arise through recombination events with commensal *Neisseria* species [29], we also determined the prevalence of Thr483 within 40 commensal *Neisseria* species in the PubMLST database. Across those 40 strains, 1.4% (25 out of 1,802) of genomes contained the T483S mutation. We also examined the conservation of the three epistatic mutations in *penA* alleles from all *Neisseria* species that contained a T483S mutation. Of these, the epistatic mutations A437V, L447V, and F462I were observed in 98% of sequences, consistent with the requirement of the epistatic mutations to preserve essential transpeptidase activity in variants harboring a T483S mutation.

Structural comparison of minimal mutant PBP2 variants

To assess the molecular impact of the epistatic mutations on PBP2, we determined the crystal structures of the tPBP2-6M, -7M, and -10M variants. All crystals grew in the same $P2_1$ crystal system as tPBP2^{FA19} [32] with two molecules in the asymmetric unit, except that tPBP2-10M crystallized with slightly altered cell dimensions (S2 Table). All three structures superimpose closely with each other and with the structures of tPBP2^{FA19} and tPBP2^{H041}, with RMS deviations in the range 0.17 to 0.47 Å for all atoms (Fig 7A). As we have reported previously [32,33,38], the conformation of the *β*3-*β*4 loop in the crystal structures differs according to the PBP2 background. In the tPBP2^{FA19} structure, the loop is in an extended conformation, and this conformation is also observed in the tPBP2-6M, -7M, and -10M variants. In contrast, the loop occupies a so-called “outbent” conformation in tPBP2^{H041}. These data show that in *apo* crystal structures at least, the mutations present in tPBP2-6M, -7M, and -10M mutants, including the 3 epistatic mutations present in tPBP2-10M, do not affect the conformation of the *β*3-*β*4 loop.

Examination of the structures around the sites of epistatic mutations reveals some interesting findings. Firstly, all three mutations are hydrophobic to hydrophobic substitutions, where two side chains have become smaller (L447V and F462I) and one larger (A437V), and all three are situated within hydrophobic core regions of the protein. Secondly, superimpositions of the variant structures with that of tPBP2^{FA19} and tPBP2^{H041} show that the hydrophobic core regions around the F462I and A437V mutations are essentially unchanged, whereas in tPBP2-10M, the structure is altered around the L447V mutation (S2 Fig). Specifically, residues on the *α*6-*β*2e loop are altered in position, as is the side chain of Phe449 (S2C Fig). This points to the L447V mutation as having the biggest effect structurally. Finally, a closer examination shows that the dihedral angles for the 446–447 peptide bond have switched from being a Ramachandran outlier in the tPBP2-6M and tPBP2-7M structures to the allowed region in tPBP2-10M (Fig 7B). This occurs in both molecules of the asymmetric unit.

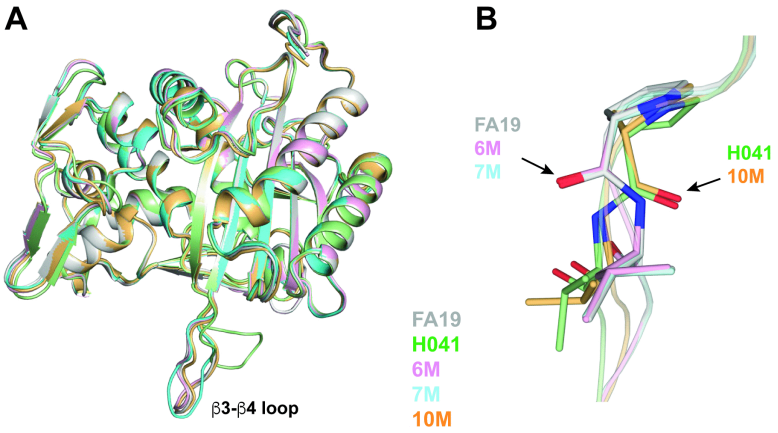

Fig 7. Stereochemistry of the peptide bond between 446 and 447 is altered by epistatic mutations. A. Superimposition of the transpeptidase domains of tPBP2 structures showing that the epistatic mutations in PBP2 do not elicit major changes in structure. **B.** As marked by arrows, the dihedral angles for 446-447 occupy a disallowed region in the crystal structures of tPBP2^{FA19} (6P53), tPBP2-6M (9Z0W), and tPBP2-7M (9Z0X), but occupy the favorable region in PBP2-10M (9Z0Y) and PBP2^{H041} (6VBC).

https://doi.org/10.1371/journal.ppat.1013721.g007

Interestingly, this bond is a Ramachandran outlier in tPBP2^{FA19} but occupies the allowed region in tPBP2^{H041}. This indicates that the L447V mutation has relieved strain present in structures that lack this mutation and is associated with higher levels of resistance.

Growth deficits conferred by key resistance mutations are compensated by the three epistatic mutations

Our data with the T483S mutation suggest that resistance mutations in PBP2 can negatively impact the essential transpeptidase function of the enzyme and thereby decrease the fitness of strains. To examine how the different resistance mutations impact strain growth (a proxy for biological fitness), we carried out quantitative growth curves of FA19 harboring key *penA* variants (Fig 8). Surprisingly, across all eight hours of growth, there were no significant differences in OD_{600} readings between FA19 *penA19* and FA19 *penA41* (Fig 8B) at any time (S3 Table). In contrast, FA19 *penA19*-10M had significantly impaired growth compared to FA19 *penA19* at 4 hours and both FA19 *penA41* and FA19 *penA19* at 8 hours (Fig 8B-8C), suggesting that while the three epistatic mutations help retain the transpeptidase function that would otherwise be damaged by T483S, the enzyme is still impaired. The T483S mutation imparts marked negative effects on fitness, as FA19 *penA19*-10M S483T (the same as the 6M construct plus three epistatic mutations) showed significantly higher growth at the 8-hour timepoint compared to FA19 *penA19*-10M (Fig 8C) and FA19 *penA19*-6M (Fig 8D). There was no significant difference between *penA19* 10M S483T and *penA41* (Fig 8D).

Discussion

In this study, we set out to understand whether the resistance mutations in the *penA41* allele from the ESC-resistant strain H041 act independently or depend on one another for their capacity to confer resistance to three β-lactam antibiotics that have been used historically to treat gonorrhea infections. By clustering the seven known resistance mutations into three groups and assessing both forward mutagenesis (incorporating *penA41* mutations into the antibiotic-susceptible *penA19* allele) and reverse mutagenesis (reverting mutations in *penA41* to their *penA19* counterparts), we determined that these mutations work together to increase resistance, but the results differed depending on which antibiotic was being tested. Overall, we observed that the MICs of the ESCs ceftriaxone and cefixime were more strongly affected by the different groups of mutations than that of penicillin G, suggesting that the mutations we examined are more important for ESC

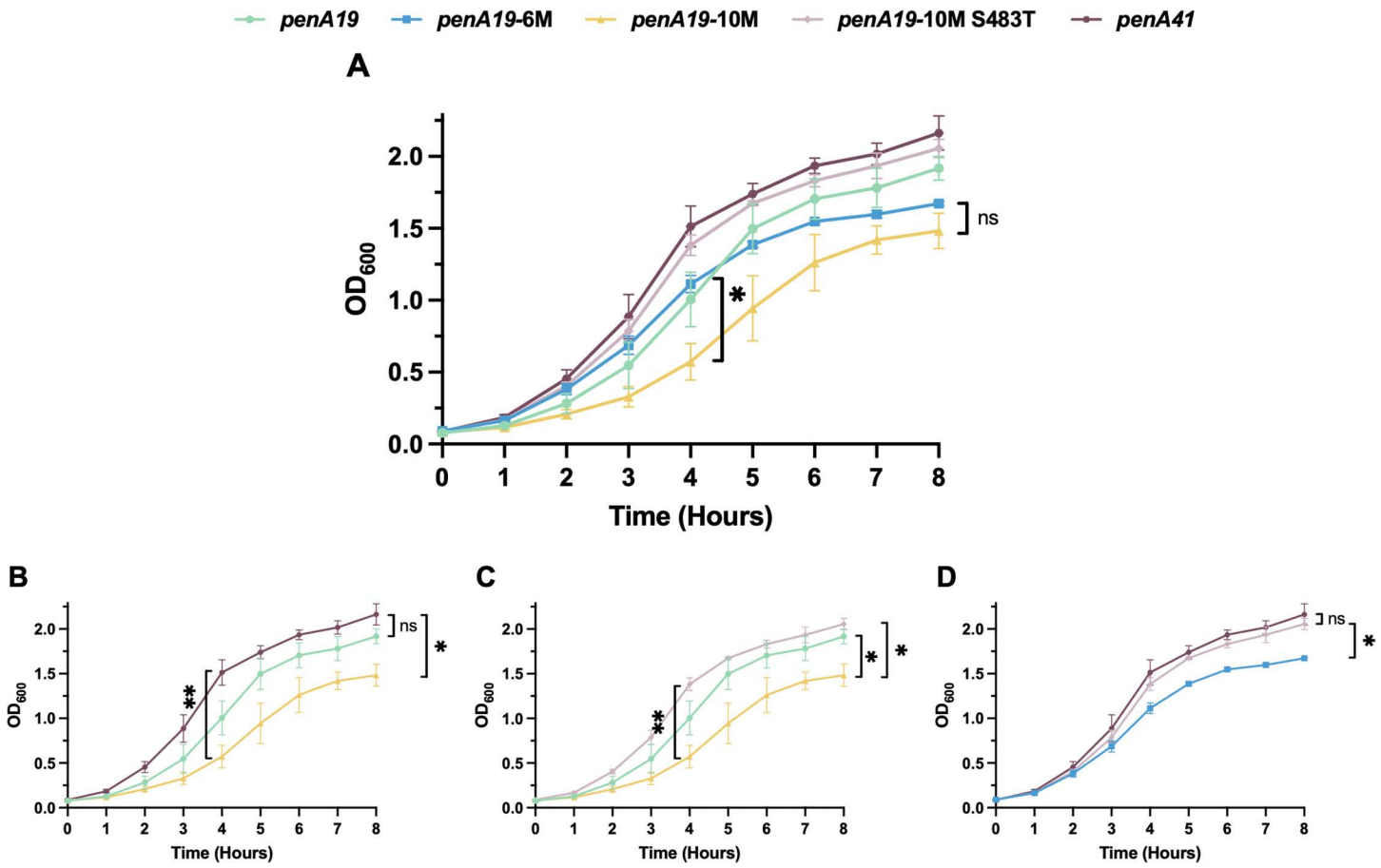

Fig 8. Quantitative growth curves of individually cultured FA19 strains with the indicated *penA* alleles. Legend for lines and symbols shown above graphs. **A.** Overlay of growth curves from all five strains tested. n = 3, with error bars showing standard deviation. At the 8-hour time point, there is no significant difference in OD_{600} between *penA19* 6M and *penA19* 10M ($p > 0.05$). **B-D**. Overlay of growth curve from the indicated strains. **B**. At the 8-hour time point, there is a significant ($p = 0.011$) difference in OD between FA19 *penA41* and FA19 *penA19*-10M strains. At all time points tested, there is no significant difference between *penA19* and *penA41* ($p > 0.05$). **C.** At the 8-hour time point, there is a significant difference in OD when comparing FA19 *penA19*-10M to both FA19 *penA19* ($p = 0.042$) and FA19 *penA19*-10M S483T ($p = 0.022$). **D.** At the 8-hour time point, there is a significant ($p = 0.022$) difference in OD_{600} between FA19 *penA19*-6M and FA19 *penA19*-10M S483T strains. Statistical significance was calculated using repeated-measures 2-way ANOVA with Geisser-Greenhouse correction and Tukey's multiple comparisons.

https://doi.org/10.1371/journal.ppat.1013721.g008

resistance than penicillin G resistance. We also uncovered a unique dependence of one of the mutations, T483S, on three epistatic mutations in a region on the opposite side of the molecule that have no impact on resistance but are required to support strain growth. The crystal structures of tPBP2-6M, -7M, and -10M revealed that the unfavorable backbone dihedral angles at residues 446–447 are relieved by the three epistatic mutations in tPBP2-10M, suggesting that this conformational change is important in maintaining function of PBP2 variants containing the T483S mutation. Lastly, quantitative growth curves show that despite the presence of the epistatic mutations, the *penA19*-10M allele still carries a strong fitness cost, because reversion of Ser483 back to threonine increases the growth of the strain to the same levels as FA19 and FA19 *penA41*. Taken together, these data suggest a complex interplay between mutations that increase resistance with other mutations that play a supporting role in maintaining essential transpeptidase function.

Our results revealed two interesting observations. First, there was a marked difference between the impact of the mutations on the MICs of the ESCs relative to the MIC_{PEN}. For example, incorporating the β3-β4 loop mutations plus G545S or

the three α2 mutations into *penA19* had no effect on MIC_{PEN}, whereas the MICs of CRO and CFX were increased 3.5- to 7-fold. The lack of an effect of the seven mutations examined here on MIC_{PEN} suggests that they are ESC-specific, and that other mutations in *penA41* are involved in increasing the MIC_{PEN}. This is perhaps not unexpected given the structural differences in these antibiotics and the fact that the *penA41* allele evolved to confer resistance to ESCs. Interestingly, whereas the α2 mutations had no effect on the activity of penicillin in the forward direction, reverting those mutations in *penA41* decreased the MIC_{PEN} by 6-fold. These data suggest that the α2 mutations may coordinate with the penicillin-specific mutations in *penA41* but by themselves do not affect the activity of penicillin G against PBP2. Secondly, although there was some variability, reverting mutations to their *penA19* counterparts in *penA41* had larger fold differences in the MICs for ESCs compared to those when introducing them into *penA19*. This hints at synergism between mutations in the context of *penA41* that do not occur in the *penA19* background.

The capacity of a β-lactam antibiotic to inhibit a PBP is defined by the second-order rate of acylation, k_2/K_s, in which k_2 is the rate of acylation and K_s is the non-covalent binding affinity (equivalent to K_d; [43]). Thus, resistance mutations can decrease the acylation rate constant k_2, decrease the non-covalent binding affinity (i.e., increase K_s), or both. We have previously shown by isothermal titration calorimetry that ceftriaxone binds to $tPBP2^{FA19}$-S310A, an acylation-incompetent mutant, with a K_s value in the low-micromolar range, but not to $tPBP2^{H041}$-S310A [33]. We also showed that introducing the β3-β4 loop mutations individually into $tPBP2^{FA19}$-S310A increased the K_s of ceftriaxone 2- to 4-fold, G545S increased K_s by 10-fold, and introducing all three together increased the K_s > 100-fold [38]. Thus, a good portion of the decrease in the MIC_{CRO} in *penA19*-F504L/N512Y/G545S is likely due to the increase in K_s, although these mutations (particularly G545S) may also decrease k_2 for reasons described for the α2 mutations below.

In contrast to the β3-β4 loop mutations and G545S, the α2 mutations are unlikely to affect binding, since the position of the α2 helix is identical in *apo* and acylated PBP2 crystal structures [32, 33]. Instead, their effects on the MICs of ESCs in the forward direction are likely due to decreasing k_2. We suspect that the α2 helix moves towards the β3 strand during the development of the transition state and concomitant formation of the oxyanion hole (comprised of the main chain amides of Ser310 and Thr500) and then relaxes back to its original location following acylation. It therefore seems likely that these three mutations hinder the transient movement of the α2 helix during acylation, thereby lowering k_2 and decreasing acylation.

Incorporating all seven resistance mutations and the three epistatic mutations into *penA19* increased the MICs of the ESCs to 67% of those conferred by *penA41*. Identifying the remaining resistance mutations in *penA41* will be difficult for multiple reasons: a) in the absence of the mosaic background, such mutations might lower transpeptidase activity to the level that no longer supports growth; b) the changes in MIC with additional mutations may be incremental, making it difficult to select; and/or c) it may require the presence of multiple mutations that work together to increase the MIC. Nonetheless, showing the high level of resistance conferred by ten mutations (of which three do not increase resistance alone but repair the transpeptidase function) from a total of 60 mutations in *penA41* relative to *penA19* provides a framework for understanding the complexities of resistance conferred by mutations in PBP2.

It is important to note that while most of the mutations identified here are present in other mosaic alleles, there are some important differences. For example, FC428 is an internationally spreading ceftriaxone-resistant clone that has a lower MIC_{CRO} than H041 (0.5 μg/mL vs 2–4 μg/mL for H041) [39]. FC428 harbors the *penA60* mosaic allele that contains 48 mutations compared to *penA19*; notably, six of the seven mutations investigated here are found in *penA60*, with the seventh (V316P) mutated to a different amino acid (V316T). Additionally, F89 (MIC_{CRO} = 1–2 μg/ml) lacks the T483S and V316P/T mutations but has an A501P mutation just downstream of the KTG motif [44]. Both PBP2 variants contain the three epistatic mutations. It seems likely that the mosaic background is more conducive to acquiring new mutations than *penA19* or similar alleles, and single mutations may arise spontaneously in the presence of selective pressure that further increase resistance.

The T483S mutation is an enigma. In *penA19*-6M with the three epistatic mutations, it increases the MIC_{CRO} by ~2.5-fold, and when reverted in *penA41*, decreases the MIC_{CRO} by 4-fold. Yet, for T483S to be tolerated by the cell in the

penA19-6M background, it requires the three epistatic residues, presumably because they restore the transpeptidase function of PBP2 that is otherwise lost when the T483S mutation is present. This is even more remarkable given that Thr to Ser is a highly conservative mutation, amounting to only loss of a methyl on the side chain. In antibiotic-bound structures of tPBP2^{FA19}, Thr483 is close to the active site, where its side chain occupies the space between Thr498, the dihydrothiazine ring of ESCs, and Ser362 of the SxN motif (Fig 9A), and it forms a hydrogen bond with Thr498. Thr498 is important for catalysis because its side chain rotates to engage the carboxylate of bound ceftriaxone/cefixime [32]. Interestingly, the same hydrogen bond can form when 483 is a Ser (*i.e.,* in PBP2^{H041}), as observed in the crystal structures of PBP2^{H041} in complex with cefoperazone or piperacillin [45] (Fig 9B). Hence, these data point to the absence of the methyl group in Ser483 as being key for resistance rather than the hydroxyl. As one potential mechanism for how it might contribute to resistance, increased flexibility of the side chain imparted by loss of the methyl makes formation of the hydrogen bond with Thr498 less favorable with Ser compared to Thr. In turn, this makes it more difficult to form the productive state for acylation by cephalosporins.

Although it cannot be proven directly in the absence of a biochemical assay for PBP2, we suspect that introduction of the T483S mutation into PBP2 decreases the transpeptidase activity of the protein below the viable threshold for growth and that this is restored by the epistatic mutations. Since PBP2-7M still binds ^{14}C penicillin G at a level consistent with the effects of T483S on resistance and because the epistatic mutations are located 22–28 Å away, their ability to preserve transpeptidase function is unlikely to involve direct contact with the active site. This suggests that they work allosterically via communication through the protein framework. It is interesting that all three residues are within hydrophobic cores, where alteration of side chains could perturb the surrounding environment. It is also notable that two of the mutations, A437V and F462I, pack within a hydrophobic core shared by α2, the helix that contains the Ser310 nucleophile at its

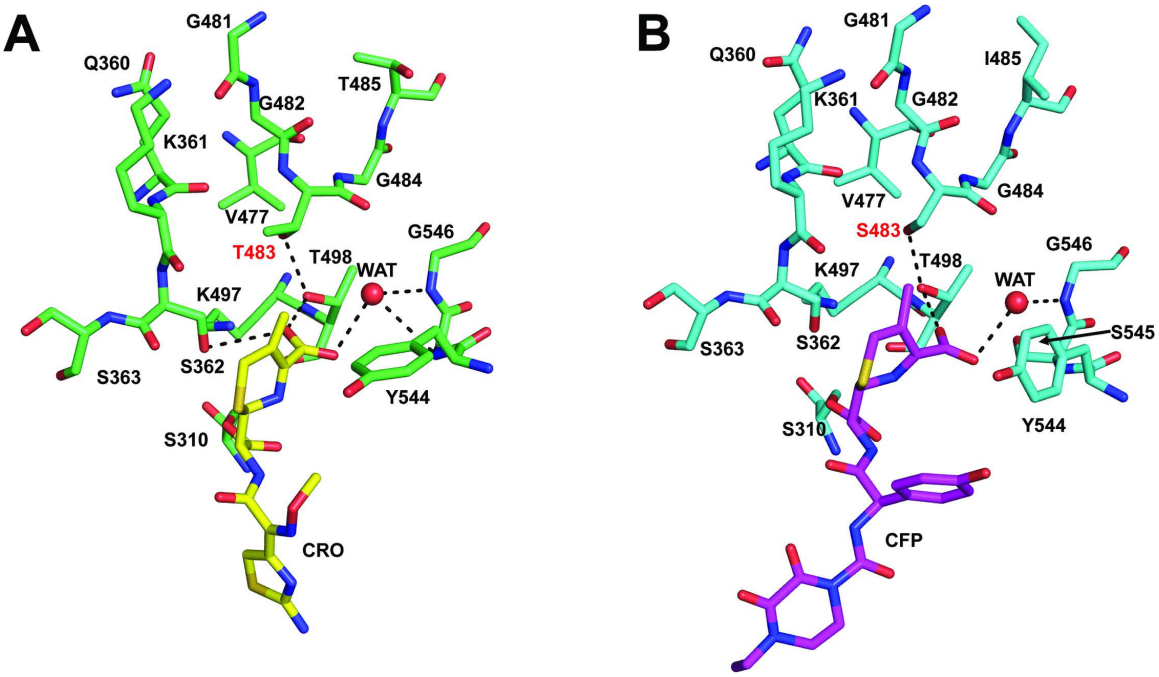

Fig 9. Thr483 and Ser483 have similar packing environments in crystal structures of PBP2 and the hydrogen bond with Thr498 is preserved. **A.** Environment around Thr483 in the crystal structure of PBP2^{FA19} (green bonds) bound by ceftriaxone (CRO, yellow bonds; 6P54) [32]. **B.** Environment around Ser483 in the crystal structure of PBP2^{H041} (cyan bonds) bound by cefoperazone (CFP, purple bonds; 8VEN) [45]. For both panels, potential hydrogen bonds are indicated by dashed lines and waters are indicated by red spheres.

https://doi.org/10.1371/journal.ppat.1013721.g009

N-terminal end. Presumably, any structural differences elicited by these two mutations are too small in magnitude to be detected by X-ray crystallography, because all structures overlap closely around these residues (S2 Fig). The situation is clearer for the L447V mutation, because the dihedral angles of the 446–447 peptide bond have switched from being in the unfavorable region of the Ramachandran plot in the structures of tPBP2^{FA19}, tPBP2-6M and tPBP2-7M to being allowed in tPBP2-10M and the same as tPBP2^{H041} (Fig 8). Consequently, there are some structural alterations around the L447V mutation, including shift of the *α*6-*β*2e loop and of the Phe449 side chain (S2C Fig). How these changes might affect Ser483 is unclear, however, since the position of this residue is similar in all structures (S3 Fig).

Quantitative growth curves in isogenic strains (with only the *penA* allele being altered) serve as a proxy for overall strain fitness and transpeptidase activity of PBP2 [46]. Surprisingly, we observed no significant difference in growth in GCB medium between FA19 and FA19 *penA41* across all timepoints tested, despite having shown previously that the *penA41* allele conferred a significant growth defect to FA19 [47]. One possibility for this difference is that the current experiments utilized a different lot of proteose peptone; indeed, the optical density at 600 nm for FA19 after 8 hours of growth reached >2, whereas it reached ~1.0 in previous experiments. This difference may suggest that certain nutrients in different lots of proteose peptone #3 could alter growth of strains with mosaic alleles, although further experimentation to test this is warranted. Interestingly, experiments by Zhou *et al.* [46] showed there was no difference in *in vitro* growth rates in GCB of isogenic strains harboring *penA10*, which is found in strains with reduced ESC susceptibility, or *penA60*, which is found in circulating strains such as FC428. However, the isogenic strain with *penA60* grew better than the strain with *penA10* when either palmitic acid or lithocholic acid was added to the growth medium. These data suggest a complex relationship between the *penA* allele and the composition of the growth medium that is not fully understood.

Conclusion

The results presented here reveal a complex and delicate balance between function and antibiotic resistance during remodeling of an essential enzyme. Because of the structural mimicry between β-lactam antibiotics and the acyl-D-Ala-D-Ala, the bacteria must alter residues that can discriminate between antibiotic and substrate. These changes very often come with a cost in terms of enzymatic function and thereby exert a fitness cost, which is very evident from our results described here. It is likely that PBP-mediated ESC resistance at the level seen with *penA41* (~400-fold increase compared to FA19) is unique to naturally competent organisms such as *N. gonorrhoeae*, as incorporating and maintaining multiple iterative resistance mutations in an antibiotic-susceptible background over time would be very difficult. This is also supported by the historical appearance of new mosaic *penA* alleles that confer increasing levels of resistance; once the mosaic background was present, the selective pressure exerted by ESCs drove additional mutations.

Methods

Materials

Ceftriaxone sodium salt hemiheptahydrate and cefixime trihydrate were purchased from Thermo Fisher. Penicillin G sodium salt was purchased from Millipore Sigma. Other reagents such as culture media, buffers, and salts were purchased from commercial vendors.

N. gonorrhoeae strains and culturing

FA19 is an antibiotic susceptible strain of *N. gonorrhoeae* that was used as the recipient strain for our transformation experiments [48]. H041 is a highly ESC- and penicillin-resistant strain that was isolated in Japan in 2009 [30,31]. Strains were grown on Gonococcal Base Medium+ (GCB+) agar plates, which were made by supplementing GC Medium Base (Difco, BD) with Kellogg's supplements I (4 mg/mL glucose, 0.1 mg/mL L-glutamate, and 0.2 μg/mL cocarboxylase, final concentrations) and II (5 μg/mL $Fe(NO_3)_3$) [49], and an additional 0.125% (w/v) agar (Bacto, BD). For *N. gonorrhoeae* growth in liquid media, GCB broth (15 g/L Proteose Peptone #3 (Bacto, BD), 4 g/L K_2HPO_4 (Fisher), 1 g/L KH_2PO_4 (Fisher),

5 g/L NaCl (Fisher), and 1 g/L soluble potato starch (Sigma)) was supplemented with 10 mM $MgCl_2$, 20 mM sodium bicarbonate, and Kellogg's supplements I and II to make liquid GCB+. For quantitative growth curves, liquid GCB+ without sodium bicarbonate was used and cultures were grown in a 37 °C incubator with 5% CO_2 in a 50 mL tissue culture flask fitted with a gas-permeable cap.

Transformation of FA19

Piliated (P+) *N. gonorrhoeae* is naturally competent, and transformation can be achieved simply by mixing DNA and P+ cells and plating on selective medium after incubating for 5 hrs as previously described [37]. All transformants were selected on GCB agar plates containing cefixime as the selection antibiotic. The concentrations differed depending on the *penA* construct, with concentrations of cefixime slightly above the MIC_{CFX} of FA19 (0.004-0.006 μg/ml) for the β3-β4 mutant and up to 0.25 μg/ml for the *penA19*-6M, -7M, and -10M constructs. The next day, colonies were streaked onto fresh GCB plates, and after overnight growth, individual colonies from the streaks were boiled in 1X TE for 5 min, the lysate was centrifuged, and 1–2 μL was used as template for PCR as described below. All transformants were sequence verified before proceeding with MIC experiments.

Generation of *N. gonorrhoeae* strains expressing mutant *penA* sequences

DNA used to transform FA19 was either sequence-verified plasmid constructs or PCR products. For plasmid constructs, sequences were cloned into pUC18us, a vector containing the 10-bp *N. gonorrhoeae* uptake sequence (5'-GCCGTCT GAA-3'). The cloned fragment comprised sequence starting at codon-45 of the *penA* gene and ending at codon-100 of *murE*, the gene downstream of *penA* in the *Neisseria gonorrhoeae* genome. The *penA* gene contained silent restriction sites to split the sequence into 6 modules as previously described [36] (see S1 Text and S1 Fig for more information), and the extra *murE* sequence was included to ensure incorporation of mutations close to the 3'-end of the *penA* gene. The template DNA for PCR reactions was either genomic DNA from FA19, H041, and variant strains (extracted using the Promega Wizard Genomic DNA Purification Kit) or from diluted *penA* plasmid DNA. Primers were designed to incorporate specific mutations and comprised ~15 bases both before and after the desired mutations to promote annealing, with the 5'- and 3'-primers complementary to each other. For certain constructs (i.e., those that conferred small increases in resistance above that for FA19), a silent restriction site was included within the mutation primer to assist in screening of transformants. PCR reactions were carried out with Pfu or Phusion polymerase. Two PCR fragments per mutant were generated: the "upstream" fragment used 5'-*penA*_45aa_US and the 3'-mutation primer, and the "downstream" fragment used the 5'-mutation primer and the 3'-*murE*_31aa primer (S4 Table). When the mutations were too distant to incorporate with one set of mutation primers (e.g., the epistatic mutations and the *penA19*-6M and -10M constructs), two or more rounds of overlap extension were carried out. The resulting purified fragments were isolated from agarose gels using Xcluda type D tips, and the full length *penA-murE19* product was amplified by PCR using the outside primers and the upstream and downstream PCR fragments. PCR products were purified using the QIAquick PCR Purification Kit and the DNA concentrations determined on a NanoDrop One (ThermoFisher). These PCR products were used either for ligation into digested plasmid DNA or directly for transformation into *N. gonorrhoeae*. A list of FA19 strains used in this study is shown in S5 Table.

Minimum Inhibitory Concentration (MIC) determinations

On the day of the experiment, 25 mL GCB agar plates with varying concentrations of ceftriaxone, cefixime, and penicillin G (2-fold and 1.5-fold dilution series, one plate at each concentration) were poured, allowed to solidify, then dried in a 37 °C incubator for at least 2 hours. The day before, nonpiliated (P-) strains were streaked from frozen stocks onto GC agar plates, and the next day the cells were resuspended in GCB+ broth at an OD_{600} of 0.018 (~1 x 10^7 cfu). Five μL of each strain (~50,000 cfu) were spotted onto each antibiotic plate and incubated for 24 hr. Growth was defined as at least five colonies growing within the spot. MIC experiments were repeated 3 times.

Analysis of *Neisseria* species *penA* loci

PubMLST comprises a curated database of genomic sequences from *N. gonorrhoeae*, *N. meningitidis*, and 40 other *Neisseria* species [40]. From this collection, all unique *penA* genes were aligned using the Locus Explorer plugin on the site. PubMLST has multiple options for calling *penA* loci, including a defined, *N. gonorrhoeae*-only option (listed as "NG_penA") and an option containing equivalent *penA* loci across all available species within the database (listed as "NEIS1753"). As of this writing, Locus Explorer can align only 2,000 protein sequences at a time, so the 5,274 loci in the NEIS1753 category were aligned in three separate batches, and then manually compared across all three groups.

For searches on the prevalence of the T483S mutation in *Neisseria* species, we used the PubMLST database genome collection tool [40], specifying the species of interest, then searching for the NEIS1753 T483S sequence variation. For searching the other 40 *Neisseria* species for T483S alterations, we excluded both *Neisseria gonorrhoeae* and *Neisseria meningitidis* species from the genome search.

Protein expression and purification

We previously reported the cloning of a TPase domain construct (designated by the prefix "t") that we use for structural and biochemical investigations of PBP2 variants [32,33,50]. Omission of the N-terminal pedestal domain does not alter second-order rates of acylation for β-lactam antibiotics [50]. DNA encoding the truncated *penA19* construct containing the 10 mutations in the 10M variant was synthesized *de novo* (GenScript, Piscataway, NJ) and cloned in-frame into the pMAL-C2KV vector [24]. This expresses tPBP2 as an N-terminal hexa-histidine–tagged fusion with maltose-binding protein, separated by a tobacco etch virus (TEV) protease site. The tPBP2-6M and -7M variants were then generated by site-directed mutagenesis of *penA19*-10M using the QuikChange Lightning kit (Agilent, Santa Clara, CA). All constructs were confirmed by Sanger sequencing. The resulting plasmids were transformed into *Escherichia coli* BL21 (DE3) cells and proteins expressed and purified as described previously [32]. As a final purification step, the protein was eluted from a 5 mL HiTrap SP FF cation-exchange column (GE Healthcare, Piscataway, NJ) equilibrated in TG buffer (20 mM Tris-HCl, pH 8.0, 10% glycerol) using a gradient of 0–500 NaCl. Fractions containing the tPBP2 variants were pooled, concentrated, and either used immediately or aliquoted and stored at −80°C.

Structure determination

Crystals of tPBP2-6M, -7M and -10M were generated by the sitting-drop vapor diffusion method in 96-well plate format, following published protocols (Singh, 2019). Prior to crystallization, proteins were concentrated to 13 mg/ml in the same buffer as eluted from the cation-exchange column. After incubation at 18 °C, crystals appeared after 3–4 days with wells containing 32−40% PEG 600 buffered with 0.1 M CHES at pH 9−10. These exhibited a similar plate morphology as crystals as $tPBP2^{FA19}$ and are in the same $P2_1$ space group with two molecules in the asymmetric unit. Diffraction data from cryo-cooled crystals were collected at the SER-CAT beamlines at the Advanced Photon Source in Argonne, IL. Data from crystals of tPBP2-6M and tPBP2-7M data were collected at a wavelength of 1.0 Å on an Eiger 16M detector at the ID-22 beamline. 360° of data were collected in 0.25° oscillations at a crystal-to-detector distance of 262 mm (tPBP2-7M) or 280 mm (tPBP2-6M). Data from tPBP2-10M crystals were collected at the BM-22 beamline on a MAR MX300-HS detector. 360° data were collected in 1° increments at a crystal-to-detector distance of 180 mm. After data processing using HKL2000 [51], structures were solved by simple refinement against the $tPBP2^{FA19}$ structure (PDB ID 6P53; [32]) or in the case of tPBP2-10M, by molecular replacement using PHASER [52] using the same starting model. The mutations were introduced into each of the three models by inspecting |Fo|−|Fc| difference electron density maps and followed by iterative cycles of model building and refinement using COOT [53] and REFMAC [54]. Molecule B is used for the structural comparisons since its β3-β4 loop is ordered, compared to it being disordered in molecule A [38].

Acylation rate determination of mutant tPBP2 constructs

The second-order rate constants (k_2/K_s) of acylation with [^{14}C]penicillin G (Moravek, Brea, CA) for the PBP2 variants were determined using purified protein, as described previously [24]. The k_2/K_s values for ceftriaxone and cefixime were determined indirectly by determining the concentrations of the cephalosporins that inhibited the binding of [^{14}C]penicillin G by 50% [37,43].

Quantitative growth curves

To generate the FA19 strains used in quantitative growth curves, the full *penA* genes from each minimal mutant construct and FA19 *penA41* were amplified by PCR with 5'-*penA*_45aa_US and 3'-*murE*_31aa primers by colony PCR or genomic DNA. The PCR products were validated by DNA sequencing (GENEWIZ, Azenta Life Sciences), then transformed into the same piliated FA19 stock on the same day. Quantitative growth curves as a measure of fitness were done similarly as described previously [47]. Briefly, after growing overnight on GCB+ agar plates, P- strains of *N. gonorrhoeae* were resuspended in GCB+ broth without sodium bicarbonate. The resuspended cultures were used to inoculate 10 mL of GCB+ broth without sodium bicarbonate to a starting OD_{600} of 0.08 in 50 mL tissue culture flasks (BioLite, ThermoFisher). The flasks were grown in a CO_2 incubator at 180 rpm for a total of 8 hours, with the OD_{600} measured every hour. At the end of the incubation, a sterile loop was dipped in each culture and streaked individually on GCB+ agar plates and assessed for potential culture contamination. Experiments were repeated at least 3 times.

Supporting information

S1 Fig. Location of the mod3^{H041} mutations relative to the T483S mutation in H041. The top panel shows the junctions of the different modules in *penA19* and the silent restriction sites used to make the constructs as described in Tomberg *et al* 2013. The solid line at the end of the *penA* genes represents downstream sequence to facilitate recombination. The number of mutations in *penA41* in each module is shown below the *penA41* schematic, and the location of the seven resistance mutations are marked with a red *. The bottom panel shows an expanded view of mod3 with the amino acids from PBP2^{FA19} and PBP2^{H041}. The 13 mutations are highlighted in blue (non-essential mutations), purple (essential mutations), and red (T483S resistance mutation).
(TIF)

S2 Fig. Molecular packing around the epistatic mutations in PBP2 in the *apo* crystal structures of tPBP2^{FA19} (grey; 6P53), tPBP2-6M (pink; 9Z0W), tPBP2-7M (cyan; 9Z0X), tPBP2-10M (orange; 9Z0Y) and tPBP2^{H041} (green; 6VBC). A. F462I: In tPBP2^{FA19}, tPBP2-6M and tPBP2-7M, Phe462 packs within a hydrophobic core and little changes structurally when the residue is mutated to Ile in tPBP2-10M and tPBP2^{H041}. Note the proximity of this position to α2. B. A437V: Similar to F462I, the hydrophobic environment around this residue is unchanged when mutated from Ala to Val. C. L447V: In contrast to F462I and A437V, there are structural differences around this residue in tPBP2^{FA19}, tPBP2-6M and tPBP2-7M compared to tPBP2-10M and tPBP2^{H041}. Specifically, the α6-β2e loop has shifted in tPBP2-10M and tPBP2^{H041} and the side chain of Phe449 moves away from the mutation site. Such changes are likely the result of the peptide bond between residues 446 and 447 switching from a Ramachandran outlier in tPBP2^{FA19}, tPBP2-6M and tPBP2-7M to occupying the favorable region in tPBP2-10M and tPBP2^{H041}.
(TIF)

S3 Fig. Relative positions of the side chain at position 484. Superimpositions of the apo crystal structures of tPBP2^{FA19} (grey; 6P53), tPBP2-6M (pink; 9Z0W), tPBP2-7M (cyan; 9Z0X), tPBP2-10M (orange; 9Z0Y) and tPBP2^{H041} (green; 6VBC) are shown.
(TIF)

S1 Text. Identification of penA41 mutations that support the viability of penA19-7M.
(DOCX)

S1 Table. Mod3^{H041} mutations introduced into *penA19*-7M or reverted to *penA19* counterparts in *penA19*-7M+-mod3^{H041} or *penA19*-13M. See S1 Fig for the location of the individual mutations. The DNA constructs with the indicated mutations were transformed into FA19 and colonies were selected on 0.1 μg/ml cefixime. The right column indicates whether the construct was able to transform FA19 with all the mutations intact. See S1 Text for further details.
(DOCX)

S2 Table. Crystallographic data collection and model refinement statistics for the *apo* crystal structures of tPBP2-6M, -7M, and 10M variants.
(DOCX)

S3 Table. Significant differences between different growth curves for each hr in Figure 9. For all time points and strains, statistical significance was calculated using repeated-measures 2-way ANOVA with Geisser-Greenhouse correction and Tukey's multiple comparisons. The table contains only those comparisons with significant differences. Any comparisons not present were considered non-significant (adjusted p value > 0.05).
(DOCX)

S4 Table. Primers for *N. gonorrhoeae* variant strain generation. The outside primers used for cloning and/or PCR amplification for transformations are shown. The 10-bp uptake sequence (US) is bolded in each primer to which it was added, and restriction sites at the start of primers for use in ligation cloning are underlined. Specific primer sequences used for site-directed mutagenesis primers will be provided upon request.
(DOCX)

S5 Table. *N. gonorrhoeae* strains used in this study. The strains were constructed as outlined in Methods. Forward mutations (introducing mutations from *penA41* into *penA19*) are shown in green, whereas reverse mutations (reverting a mutation in *penA41* to the residue in *penA19*) are shown in red.
(DOCX)

Acknowledgments

Use of the Advanced Photon Source was supported by the U.S. Department of Energy, Office of Science, Office of Basic Energy Sciences, under Contract No. W-31–109-ENG-38. Data were collected at Southeast Regional Collaborative Access Team (SER-CAT) 22-ID and 22-BM beam lines at the Advanced Photon Source, Argonne National Laboratory. Supporting institutions may be found at www.ser-cat.org/members.html.

Author contributions

Conceptualization: Christopher Davies, Robert A Nicholas.

Data curation: Marissa M Bivins, Joshua Tomberg, Christopher Davies.

Formal analysis: Marissa M Bivins, Joshua Tomberg, Avinash Singh, Sandeepchowdary Bala, Christopher Davies, Robert A Nicholas.

Funding acquisition: Christopher Davies, Robert A Nicholas.

Investigation: Marissa M Bivins, Joshua Tomberg, Madeleine Bagshaw, Avinash Singh.

Methodology: Marissa M Bivins, Joshua Tomberg, Madeleine Bagshaw, Avinash Singh.

Project administration: Marissa M Bivins, Christopher Davies, Robert A Nicholas.

Resources: Christopher Davies, Robert A Nicholas.

Supervision: Christopher Davies, Robert A Nicholas.

Validation: Marissa M Bivins.

Visualization: Sandeepchowdary Bala, Christopher Davies, Robert A Nicholas.

Writing – original draft: Marissa M Bivins.

Writing – review & editing: Marissa M Bivins, Joshua Tomberg, Christopher Davies, Robert A Nicholas.

References

1. Unemo M, Seifert HS, Hook EW, Hawkes S, Ndowa F, Dillon JR. Gonorrhoea. Nat Rev Dis Primers. 2019;5(1):79. https://doi.org/10.1038/s41572-019-0128-6 PMID: 31754194
2. CDC. Sexually transmitted infections surveillance, 2024 (provisional). Centers for Disease Control and Prevention. 2024. Available from: https://www.cdc.gov/sti-statistics/annual/index.html
3. Lovett A, Duncan JA. Human immune responses and the natural history of *Neisseria gonorrhoeae* infection. Front Immunol. 2019;9:3187. https://doi.org/10.3389/fimmu.2018.03187 PMID: 30838004
4. Chang S-X, Chen K-K, Liu X-T, Xia N, Xiong P-S, Cai Y-M. Cross-sectional study of asymptomatic *Neisseria gonorrhoeae* and *Chlamydia trachomatis* infections in sexually transmitted disease related clinics in Shenzhen, China. PLoS One. 2020;15(6):e0234261. https://doi.org/10.1371/journal.pone.0234261 PMID: 32516318
5. Farley TA, Cohen DA, Elkins W. Asymptomatic sexually transmitted diseases: the case for screening. Prev Med. 2003;36(4):502–9. https://doi.org/10.1016/s0091-7435(02)00058-0 PMID: 12649059
6. Eisinger RW, Erbelding E, Fauci AS. Refocusing research on sexually transmitted infections. J Infect Dis. 2020;222(9):1432–4. https://doi.org/10.1093/infdis/jiz442. PMID: 31495889
7. Unemo M, Jensen JS. Antimicrobial-resistant sexually transmitted infections: gonorrhoea and *Mycoplasma genitalium*. Nat Rev Urol. 2017;14(3):139–52. https://doi.org/10.1038/nrurol.2016.268 PMID: 28072403
8. Unemo M, Ross J, Serwin AB, Gomberg M, Cusini M, Jensen JS. 2020 European guideline for the diagnosis and treatment of gonorrhoea in adults. Int J STD AIDS. 2020;:956462420949126. https://doi.org/10.1177/0956462420949126 PMID: 33121366
9. Fifer H, Doumith M, Rubinstein L, Mitchell L, Wallis M, Singh S, et al. Ceftriaxone-resistant *Neisseria gonorrhoeae* detected in England, 2015-24: an observational analysis. J Antimicrob Chemother. 2024;79(12):3332–9. https://doi.org/10.1093/jac/dkae369 PMID: 39417254
10. Lahra MM, Martin I, Demczuk W, Jennison AV, Lee KI, Nakayama SI, et al. Cooperative recognition of internationally disseminated ceftriaxone-resistant *Neisseria gonorrhoeae* strain. Emerg Infect Dis. 2018;24(4):735–40. https://doi.org/10.3201/eid2404.171873 PMID: 29553335
11. Unemo M, Golparian D, Shafer WM. Challenges with gonorrhea in the era of multi-drug and extensively drug resistance - are we on the right track? Expert review of anti-infective therapy. 2014;12(6):653–6. https://doi.org/10.1586/14787210.2014.906902 PMID: 24702589
12. Unemo M, Del Rio C, Shafer WM. Antimicrobial resistance expressed by *Neisseria gonorrhoeae*: a major global public health problem in the 21st century. Microbiol Spectr. 2016;4(3):10.1128/microbiolspec.EI10-0009–2015. https://doi.org/10.1128/microbiolspec.EI10-0009-2015 PMID: 27337478
13. Workowski KA, Bachmann LH, Chan PA, Johnston CM, Muzny CA, Park I. Sexually transmitted infections treatment guidelines, 2021. MMWR Recomm Rep. 2021;70(4):1–187. https://doi.org/10.15585/mmwr.rr7004a1 PMID: 34292926
14. Macheboeuf P, Contreras-Martel C, Job V, Dideberg O, Dessen A. Penicillin binding proteins: key players in bacterial cell cycle and drug resistance processes. FEMS Microbiol Rev. 2006;30(5):673–91. https://doi.org/10.1111/j.1574-6976.2006.00024.x PMID: 16911039
15. Sauvage E, Kerff F, Terrak M, Ayala JA, Charlier P. The penicillin-binding proteins: structure and role in peptidoglycan biosynthesis. FEMS Microbiol Rev. 2008;32(2):234–58. https://doi.org/10.1111/j.1574-6976.2008.00105.x PMID: 18266856
16. Barbour AG. Properties of penicillin-binding proteins in *Neisseria gonorrhoeae*. Antimicrob Agents Chemother. 1981;19(2):316–22. https://doi.org/10.1128/AAC.19.2.316 PMID: 6812490
17. Ropp PA, Nicholas RA. Cloning and characterization of the ponA gene encoding penicillin-binding protein 1 from *Neisseria gonorrhoeae* and *Neisseria meningitidis*. J Bacteriol. 1997;179(8):2783–7. https://doi.org/10.1128/jb.179.8.2783-2787.1997 PMID: 9098083
18. Taguchi A, Welsh MA, Marmont LS, Lee W, Sjodt M, Kruse AC, et al. FtsW is a peptidoglycan polymerase that is functional only in complex with its cognate penicillin-binding protein. Nat Microbiol. 2019;4(4):587–94. https://doi.org/10.1038/s41564-018-0345-x PMID: 30692671
19. Sjodt M, Rohs PDA, Gilman MSA, Erlandson SC, Zheng S, Green AG, et al. Structural coordination of polymerization and crosslinking by a SEDS-bPBP peptidoglycan synthase complex. Nat Microbiol. 2020;5(6):813–20. https://doi.org/10.1038/s41564-020-0687-z PMID: 32152588
20. Li Y, Gong H, Zhan R, Ouyang S, Park K-T, Lutkenhaus J, et al. Genetic analysis of the septal peptidoglycan synthase FtsWI complex supports a conserved activation mechanism for SEDS-bPBP complexes. PLoS Genet. 2021;17(4):e1009366. https://doi.org/10.1371/journal.pgen.1009366 PMID: 33857142

21. Ghuysen J-M, Hakenbeck R. Biochemistry of the penicilloyl serine transferases. Bacterial Cell Walls. Amsterdam: Elsevier Science B.V.; 1994. p. 103–29.
22. Ghuysen JM. Serine beta-lactamases and penicillin-binding proteins. Annu Rev Microbiol. 1991;45:37–67. https://doi.org/10.1146/annurev.mi.45.100191.000345 PMID: 1741619
23. Ropp PA, Hu M, Olesky M, Nicholas RA. Mutations in ponA, the gene encoding penicillin-binding protein 1, and a novel locus, penC, are required for high-level chromosomally mediated penicillin resistance in *Neisseria gonorrhoeae*. Antimicrob Agents Chemother. 2002;46(3):769–77. https://doi.org/10.1128/AAC.46.3.769-777.2002 PMID: 11850260
24. Powell AJ, Tomberg J, Deacon AM, Nicholas RA, Davies C. Crystal structures of penicillin-binding protein 2 from penicillin-susceptible and -resistant strains of *Neisseria gonorrhoeae* reveal an unexpectedly subtle mechanism for antibiotic resistance. J Biol Chem. 2009;284(2):1202–12. https://doi.org/10.1074/jbc.M805761200 PMID: 18986991
25. Spratt BG. Hybrid penicillin-binding proteins in penicillin-resistant strains of *Neisseria gonorrhoeae*. Nature. 1988;332(6160):173–6. https://doi.org/10.1038/332173a0 PMID: 3126399
26. Ameyama S, Onodera S, Takahata M, Minami S, Maki N, Endo K, et al. Mosaic-like structure of penicillin-binding protein 2 Gene (penA) in clinical isolates of *Neisseria gonorrhoeae* with reduced susceptibility to cefixime. Antimicrob Agents Chemother. 2002;46(12):3744–9. https://doi.org/10.1128/AAC.46.12.3744-3749.2002 PMID: 12435671
27. Tanaka M, Nakayama H, Tunoe H, Egashira T, Kanayama A, Saika T, et al. A remarkable reduction in the susceptibility of *Neisseria gonorrhoeae* isolates to cephems and the selection of antibiotic regimens for the single-dose treatment of gonococcal infection in Japan. J Infect Chemother. 2002;8(1):81–6. https://doi.org/10.1007/s101560200011 PMID: 11957125
28. Lindberg R, Fredlund H, Nicholas R, Unemo M. *Neisseria gonorrhoeae* isolates with reduced susceptibility to cefixime and ceftriaxone: association with genetic polymorphisms in penA, mtrR, porB1b, and ponA. Antimicrob Agents Chemother. 2007;51(6):2117–22. https://doi.org/10.1128/AAC.01604-06 PMID: 17420216
29. Ito M, Deguchi T, Mizutani K-S, Yasuda M, Yokoi S, Ito S-I, et al. Emergence and spread of *Neisseria gonorrhoeae* clinical isolates harboring mosaic-like structure of penicillin-binding protein 2 in Central Japan. Antimicrob Agents Chemother. 2005;49(1):137–43. https://doi.org/10.1128/AAC.49.1.137-143.2005 PMID: 15616287
30. Ohnishi M, Golparian D, Shimuta K, Saika T, Hoshina S, Iwasaku K, et al. Is *Neisseria gonorrhoeae* initiating a future era of untreatable gonorrhea?: detailed characterization of the first strain with high-level resistance to ceftriaxone. Antimicrob Agents Chemother. 2011;55(7):3538–45. https://doi.org/10.1128/AAC.00325-11 PMID: 21576437
31. Ohnishi M, Saika T, Hoshina S, Iwasaku K, Nakayama S, Watanabe H, et al. Ceftriaxone-resistant *Neisseria gonorrhoeae*, Japan. Emerg Infect Dis. 2011;17(1):148–9. https://doi.org/10.3201/eid1701.100397 PMID: 21192886
32. Singh A, Tomberg J, Nicholas RA, Davies C. Recognition of the β-lactam carboxylate triggers acylation of *Neisseria gonorrhoeae* penicillin-binding protein 2. J Biol Chem. 2019;294(38):14020–32. https://doi.org/10.1074/jbc.RA119.009942 PMID: 31362987
33. Singh A, Turner JM, Tomberg J, Fedarovich A, Unemo M, Nicholas RA, et al. Mutations in penicillin-binding protein 2 from cephalosporin-resistant *Neisseria gonorrhoeae* hinder ceftriaxone acylation by restricting protein dynamics. J Biol Chem. 2020;295(21):7529–43. https://doi.org/10.1074/jbc.RA120.012617 PMID: 32253235
34. Ghuysen JM. Bacterial active-site serine penicillin-interactive proteins and domains: mechanism, structure, and evolution. Rev Infect Dis. 1988;10(4):726–32. https://doi.org/10.1093/clinids/10.4.726 PMID: 3055171
35. Takahata S, Senju N, Osaki Y, Yoshida T, Ida T. Amino acid substitutions in mosaic penicillin-binding protein 2 associated with reduced susceptibility to cefixime in clinical isolates of *Neisseria gonorrhoeae*. Antimicrob Agents Chemother. 2006;50(11):3638–45. https://doi.org/10.1128/AAC.00626-06 PMID: 16940068
36. Tomberg J, Unemo M, Davies C, Nicholas RA. Molecular and structural analysis of mosaic variants of penicillin-binding protein 2 conferring decreased susceptibility to expanded-spectrum cephalosporins in *Neisseria gonorrhoeae*: role of epistatic mutations. Biochemistry. 2010;49(37):8062–70. https://doi.org/10.1021/bi101167x PMID: 20704258
37. Tomberg J, Unemo M, Ohnishi M, Davies C, Nicholas RA. Identification of amino acids conferring high-level resistance to expanded-spectrum cephalosporins in the penA gene from *Neisseria gonorrhoeae* strain H041. Antimicrob Agents Chemother. 2013;57(7):3029–36. https://doi.org/10.1128/AAC.00093-13 PMID: 23587946
38. Fenton BA, Tomberg J, Sciandra CA, Nicholas RA, Davies C, Zhou P. Mutations in PBP2 from ceftriaxone-resistant *Neisseria gonorrhoeae* alter the dynamics of the β3-β4 loop to favor a low-affinity drug-binding state. J Biol Chem. 2021;297(4):101188. https://doi.org/10.1016/j.jbc.2021.101188 PMID: 34529975
39. Nakayama S, Shimuta K, Furubayashi K, Kawahata T, Unemo M, Ohnishi M. New ceftriaxone- and multidrug-resistant *Neisseria gonorrhoeae* strain with a novel mosaic penA gene isolated in Japan. Antimicrob Agents Chemother. 2016;60(7):4339–41. https://doi.org/10.1128/aac.00504-16 PMID: 27067334
40. Jolley KA, Bray JE, Maiden MCJ. Open-access bacterial population genomics: BIGSdb software, the PubMLST.org website and their applications. Wellcome Open Res. 2018;3:124. https://doi.org/10.12688/wellcomeopenres.14826.1 PMID: 30345391
41. Chen M, Shao Y, Luo J, Yuan L, Wang M, Chen M, et al. Penicillin and cefotaxime resistance of quinolone-resistant *Neisseria meningitidis* clonal complex 4821, Shanghai, China, 1965-2020. Emerg Infect Dis. 2023;29(2):341–50. https://doi.org/10.3201/eid2902.221066 PMID: 36692352

42. Unitt A, Maiden M, Harrison O. Characterizing the diversity and commensal origins of penA mosaicism in the genus Neisseria. Microb Genom. 2024;10(2). https://doi.org/10.1099/mgen.0.001209 PMID: 38381035

43. Frere JM, Nguyen-Disteche M, Coyette J, Joris B. Mode of action: interaction with the penicillin binding proteins. Glasgow: Chapman & Hall; 1992.

44. Unemo M, Golparian D, Nicholas R, Ohnishi M, Gallay A, Sednaoui P. High-level cefixime- and ceftriaxone-resistant *Neisseria gonorrhoeae* in France: novel penA mosaic allele in a successful international clone causes treatment failure. Antimicrob Agents Chemother. 2012;56(3):1273–80. https://doi.org/10.1128/AAC.05760-11 PMID: 22155830

45. Turner JM, Stratton CM, Bala S, Cardenas Alvarez M, Nicholas RA, Davies C. Ureidopenicillins are potent inhibitors of penicillin-binding protein 2 from multidrug-resistant *Neisseria gonorrhoeae* H041. ACS Infect Dis. 2024;10(4):1298–311. https://doi.org/10.1021/acsinfecdis.3c00713 PMID: 38446051

46. Zhou K, Chen S-C, Yang F, van der Veen S, Yin Y-P. Impact of the gonococcal FC428 penA allele 60.001 on ceftriaxone resistance and biological fitness. Emerg Microbes Infect. 2020;9(1):1219–29. https://doi.org/10.1080/22221751.2020.1773325 PMID: 32438866

47. Vincent LR, Kerr SR, Tan Y, Tomberg J, Raterman EL, Dunning Hotopp JC, et al. In vivo-selected compensatory mutations restore the fitness cost of mosaic pena alleles that confer ceftriaxone resistance in *Neisseria gonorrhoeae*. mBio. 2018;9(2):e01905-17. https://doi.org/10.1128/mBio.01905-17 PMID: 29615507

48. Guymon LF, Walstad DL, Sparling PF. Cell envelope alterations in antibiotic-sensitive and-resistant strains of *Neisseria gonorrhoeae*. J Bacteriol. 1978;136(1):391–401. https://doi.org/10.1128/jb.136.1.391-401.1978 PMID: 101519

49. Kellogg DS Jr, Peacock WI Jr, Deacon WE, Brown L, Pirkle DI. *Neisseria Gonorrhoeae*. I. Virulence genetically linked to clonal variation. J Bacteriol. 1963;85(6):1274–9. https://doi.org/10.1128/jb.85.6.1274-1279.1963 PMID: 14047217

50. Fedarovich A, Cook E, Tomberg J, Nicholas RA, Davies C. Structural effect of the Asp345a insertion in penicillin-binding protein 2 from penicillin-resistant strains of *Neisseria gonorrhoeae*. Biochemistry. 2014;53(48):7596–603. https://doi.org/10.1021/bi5011317 PMID: 25403720

51. Otwinowski Z, Minor W. Processing of X-ray diffraction data collected in oscillation mode. Methods Enzymol. 1997;276:307–26. https://doi.org/10.1016/S0076-6879(97)76066-X PMID: 27754618

52. McCoy AJ, Grosse-Kunstleve RW, Adams PD, Winn MD, Storoni LC, Read RJ. Phaser crystallographic software. J Appl Crystallogr. 2007;40(Pt 4):658–74. https://doi.org/10.1107/S0021889807021206 PMID: 19461840

53. Emsley P, Lohkamp B, Scott WG, Cowtan K. Features and development of Coot. Acta Crystallographica Section D, Biological Crystallography. 2010;66(4):486–501. https://doi.org/10.1107/S0907444910007493 PMID: 20383002

54. Murshudov GN, Vagin AA, Dodson EJ. Refinement of macromolecular structures by the maximum-likelihood method. Acta Crystallogr D Biol Crystallogr. 1997;53(Pt 3):240–55. https://doi.org/10.1107/S0907444996012255 PMID: 15299926